

## USE OF GROUND PENETRATING RADAR AND STANDARD GEOPHYSICAL METHODS TO EXPLORE THE SUBSURFACE

RAFFAELE PERSICO<sup>1</sup> & SEBASTIANO D'AMICO<sup>2</sup>

<sup>1</sup> INSTITUTE FOR ARCHAEOLOGICAL AND MONUMENTAL HERITAGE OF THE NATIONAL RESEARCH  
COUNCIL (IBAM-CNR), LECCE, ITALY  
R.PERSICO@IBAM.CNR.IT

<sup>2</sup> UNIVERSITY OF MALTA, FACULTY OF SCIENCE, MSIDA, MALTA  
SEBASTIANO.DAMICO@UM.EDU.MT

### ABSTRACT

*This paper presents the results of a series of Ground Penetrating Radar (GPR) and passive seismic measurements performed in Malta in 2015, during a Short-Term Scientific Mission (STSM) funded by COST (European Cooperation in Science and Technology) Action TU1208 “Civil engineering applications of Ground Penetrating Radar.” The main purposes of the measurements were: to test the performance of an innovative reconfigurable stepped-frequency GPR prototype, recently upgraded thanks to the results of the research activities carried out in Norway during a previous TU1208 STSM; to investigate the geological conditions of some sites of historical and environmental interest; and to assess the internal status of two monuments. To the best of our knowledge, the GPR measurements carried out during this STSM constitute the first GPR investigations ever performed in Malta.*

**KEYWORDS:** Ground Penetrating Radar; Instrumentation development; Stepped frequency; Cultural heritage; Geology; Passive seismic.

### 1. INTRODUCTION

A Short-Term Scientific-Mission (STMS) entitled “Use of Ground Penetrating Radar and standard geophysical methods to explore the subsurface” was recently funded by COST (European Cooperation in Science and Technology), in the framework of the COST Action TU1208 “Civil engineering applications of Ground Penetrating Radar” activities. Raffaele Persico visited Sebastiano D’Amico in Malta, from July 13<sup>th</sup> to July 24<sup>th</sup>, 2015, and they jointly performed a series of Ground

Penetrating Radar (GPR) and passive seismic measurements in sites of historical and environmental interest.

The used radar system was an innovative reconfigurable stepped-frequency GPR prototype (Section 2). The original version of this prototype was implemented in Italy, by the Institute for Archaeological and Monumental Heritage of the National Research Council (IBAM-CNR), in cooperation with the University of Florence and the Italian company IDS Ingegneria dei Sistemi, within the research project AITECH funded by Regione Puglia ([www.aitech.net.com/ibam.html](http://www.aitech.net.com/ibam.html)) [1]. During a previous STSM funded by the COST Action TU1208, carried out in 2014, the prototype was brought to Norway and compared with commercial systems manufactured by 3d-radar [2]. Based on the results collected during that mission, the prototype was improved. The STSM in Malta represented an opportunity to test on real scenarios the improved version of the prototype.

For what concerns the passive seismic acquisitions, single station-location measurements were done.

The geology of Malta is shortly described in Section 3, whereas Section 4 is dedicated to the presentation and interpretation of the obtained results. The main objectives of our measurements were three: to test the performance of the GPR prototype, to study the geological conditions of a series of sites in Malta, and to assess the conditions of some monuments, still in Malta. In particular, we performed measurements in the Golden Bay area, in the vicinity of Ghajn Tuffieha Tower (subsection 4.1); we assessed an area close to La Ferla Cross church (subsection 4.2); we performed measurements inside Madliena tower, in Pembroke (subsection 4.3); and we surveyed the area outside the church of Santa Maria, in Birkikara (subsection 4.4). GPR and passive seismic analyses were performed also in the co-cathedral of St John patrimony of UNESCO, with the aim to test the displacement of some tombs under the floor and investigate the causes of a fracture, which is evident on one of the headstones (subsection 4.5). Measurements performed to test the performance of the improved GPR prototype are presented in subsection 4.6.

To the best of our knowledge, the GPR acquisitions carried out during this STSM constitute the first GPR investigation ever performed in Malta.

## 2. EQUIPMENT

The reconfigurable stepped-frequency GPR prototype, which was used to perform the measurements presented in this paper, is equipped with three equivalent couples of antennas, achieved by means of two series of switches along the arms of a couple of bow-tie antennas. The on and off states of the switches make electrically longer or shorter the bow-tie antennas, thus achieving efficient transmission on three different bands that overall cover the frequency range from 50 MHz to 1 GHz. Accordingly, from now on we will distinguish a couple of low-frequency antennas (with a central frequency around 120 MHz), a couple of medium-frequency antennas (with a central around 250 MHz), and a couple of high-frequency antennas (with a central frequency around 500 MHz) [3]. The prototype can gather data with the three equivalent couples of antennas during each profile acquisition, so that it is possible to obtain three B-Scans for each measurement line.

This feature of the prototype can be very useful because, as is well known, a trade-off always has to be achieved between the desired resolution of the GPR images (a better resolution is possible with higher frequencies) and the penetration depth of the GPR radiation (a deeper penetration is possible with lower frequencies). The resolution and depth of course depend also on the electromagnetic properties of the soil. As the condition of the soil and the depth of the sought targets are not always known a-priori, the large quantity of data gathered by the prototype provides robustness against these uncertainties. The same purpose might be reached with a system equipped with three separate couples of antennas. However, such a system would be necessarily larger and heavier than the prototype. Moreover, to the best of our knowledge, no commercial systems with three couples of antennas exist, but only systems with two couples of antennas at most (unless the systems equipped with antenna arrays are considered).

On the other hand, the large amount of gathered data prevents (at the moment) the visualization of the B-Scans in real time. As a possible future development, more efficient acquisition software will be developed (e.g., based on the C language, whereas the current code is written in MATLAB). This new software, along with a more powerful laptop (e.g., equipped with a parallel processor), will allow overcoming this limitation.

Another interesting and innovative feature of the reconfigurable prototype is the possibility to program the integration time of the radiated and received harmonic signals. This option can be useful in order to counteract narrow-band interferences in an efficient way. In particular, commercial stepped-frequency systems allow, at most, setting the integration time of all the radiated and received harmonic tones. This means that, if interference is recognised, it is possible to counteract it only by prolonging the integration time of all the harmonic tones, which is redundant and above all meaningfully prolongs the time required for gathering the data. In the reconfigurable prototype, instead, we have set and tested a method for recognising, in the field, the most disturbed tones (if any), and we have developed and implemented an algorithm that increases the integration times accordingly to the recorded disturbance, tone by tone. This allows to save time and prevents the measurements from becoming too long and expensive.

The algorithm for the choice of the reconfiguration times works as follows. As a first step, a preliminary B-Scan is performed, possibly coinciding with the first B-scan of interest for the GPR prospecting at hand. For each trace of this B-scan, and for each harmonic tone within the trace, N samples of the in-phase and in-quadrature (I and Q) components are retrieved and stored, and the variance of the I and Q samples is calculated as

$$\left\{ \begin{array}{l} \sigma_{I;f_k,t_h}^2 = E \left[ (I_{f_k,t_h})^2 \right] - [E(I_{f_k,t_h})]^2 \\ \sigma_{Q;f_k,t_h}^2 = E \left[ (Q_{f_k,t_h})^2 \right] - [E(Q_{f_k,t_h})]^2 \end{array} \right\} \quad (1)$$

where  $E$  indicates the algebraic average of the samples. Then, the variance  $\sigma_{f_k,t_h}^2$  of each tone is retrieved for each trace, as the algebraic average of  $\sigma_{I;f_k,t_h}^2$  and  $\sigma_{Q;f_k,t_h}^2$ . Subsequently, and conservatively, we keep the maximum of the variance for each tone, as an index representing the degree of disturbance at each frequency. Moreover we keep the quantity  $\sigma_{f_k}^2 = \max_h(\sigma_{f_k,t_h}^2)$  for each trace, which is the maximum variance over the traces for each tone; this quantity is a function of the frequency. Afterwards, by visualizing the graph of  $\sigma_f^2$  versus frequency, we can decide whether a reconfiguration of the integration time of each tone is needed or not. At this point, if we decide to apply a reconfiguration, we have just to set an integer number  $M > 1$ , which quantifies the maximum “degree” of reconfiguration needed in the case

at hand. Then, the reconfiguration code calculates a factor of enlargement for each integration time according to the formula:

$$F(k) = C_{eil} \left( M \frac{\sigma_{fx}^2}{\max_k(\sigma_{fx}^2)} \right) \quad (2)$$

where  $F$  is the factor of enlargement for the  $k^{\text{th}}$  tone and the function  $C_{eil}$  stands for the minimum integer not smaller than the argument. In other words, an enlargement time is calculated for the most disturbed tone, while the other ones are about proportionally less enlarged with the implicit care that the reconfiguration will never shorten the default integration, which is guaranteed by the  $C_{eil}$  function. Indeed, the hardware of the system does not allow an enlargement of the default integration time beyond a factor equal to 10, and therefore a subsequent “if-then” instruction saturates to 10 any value  $F > 10$ . This is because the hardware of the GPR system can prolong at most 10 times the default integration time of each harmonic tone. Let us explicitly note that the chosen algorithm is not semantically equivalent to impose that  $F$  is minor or equal to 10.

Passive seismic techniques were used to gather useful data to be compared and integrated with those obtained with the GPR prototype.

The ambient noise was recorded by using a three-component seismometer Tromino™ ([www.tromino.eu](http://www.tromino.eu)). The Tromino is a compact, lightweight and self-contained instrument; its ease of use makes it ideal to perform a large number of measurements in rugged terrains that are accessible only on foot. Time series of 20 min each were recorded at a sampling rate of 128 Hz and, by following the guidelines suggested by the SESAME project [4], these were divided into 60 non-overlapping time windows, 20-s each. The Fourier spectrum of each window was computed and smoothed, and after ‘cleaning’ the traces from spurious noise event windows, the resulting H/V, in the frequency domain, was derived by using the geometric mean of the spectral ratio obtained for each time window. The use of the H/V method was first proposed in [5] for the estimate of seismic site response. A subsequent study [6] eventually made this method widely popular as a cost-effective and reliable means of predicting the resonance frequency of a site, particularly when low shear-wave velocity layers present a sharp impedance contrast with the bedrock.

The presence of a resonance peak in the H/V ratio can be interpreted in terms of *SH*-wave resonance in soft surface layers, or in terms of the ellipticity of particle motion when the ambient noise wave train is made up predominantly of surface waves [7]. In practice, the wavefield is expected to be a combination of both types, and the H/V curve contains information about the shear wave velocity profile in shallow sediments.

### 3. THE GEOLOGY OF MALTA

The experimental results presented in this paper were obtained in several sites in Malta, as depicted in Figure 1.

The geology of the Maltese Islands is well known (see [8, 9] and references therein) and consists of four main sedimentary layers; the relief, which is largely controlled by the neotectonic pattern, is rather complex. The sedimentary sequence was deposited during the Oligocene and Miocene epochs. Starting from the oldest one, the sequence of strata consists of:



**FIG. 1** – Map showing the location of the sites where GPR and passive seismic measurements were performed during the STSM.

(i) The Lower Coralline Limestone (LCL) formation (Chattian): This is the oldest unit of rock visible above sea level. It is a hard and compact pale grey limestone, rich in coralline algae, and can be over 140 m thick. The LCL forms the sheer cliffs bordering the south-western coast of the Maltese Islands.

(ii) The Globigerina Limestone (GL) formation (Aquitanian–Langhian): This layer is made up of soft yellowish fine-grained limestone. Its thickness varies between 20 m and 200 m. The fine-grained GL is lightly cemented making this layer soft and easily cut, sculpted and eroded. It is subdivided into three sublayers: the Lower (Mlg), the Middle (Mmg) and the Upper Globigerina Limestone (Mug). These three layers are separated by two thin hard ground conglomerate layers (Mc1/Mc2), which are much harder and more resistant to erosion, and easily identified when exposed.

(iii) The Blue Clay (BC) formation (Serravallian to early Tortonian, denoted as Mbc): This layer can be considered as a continuation of the Globigerina Limestone, being composed of very fine grained sediment and containing deep water planktonic organisms. The main difference is the higher clay mineral content which gives this layer the banded bluish grey colour. The mix of clay between the lime rich sedimentary grains prevent the binding of the particles hence it is the softest layer of all and is eroded very quickly with rain water. Very often it provokes landslides and in various parts of the islands it forms 45° talus slopes over the underlying strata. Its depth varies between 20 m and 70 m, thinning notably from west to east of the archipelago [8]. Above the Blue Clay Formation there is a thin layer of bioclastic limestone named the Greensand Formation (Mgg). This layer varies from 1 m to 11 m in depth and is present only in a limited number of areas of the islands.

(iv) The Upper Coralline Limestone (UCL) formation (late Tortonian–early Messinian): this is the uppermost, and youngest layer and was formed in very similar conditions as the Lower Coralline Limestone, in shallow waters. This hard pale grey layer can reach thicknesses of more than 160 m in certain parts of the islands. As with the LCL, the layer presents a variety of facies ranging from reef limestone to cross-bedded sands and fine-grained muds. No marine sediments younger than the UCL are found on the islands, indicating that the time of uplift of the islands above sea level together with the northern flank of the Sicily Channel Rift [9] occurred around 6 Ma ago. This uplift coincided with

the closure and partial desiccation of the Mediterranean during the Messinian. Some patchy deposits of the Pleistocene epoch containing remains of terrestrial fauna were laid down on land by fluvial action and are mostly found near shorelines and in caves. Over approximately the eastern half of the island of Malta, the BC and UCL layers are absent, the GL being the outcropping layer. The western half of Malta, together with the island of Gozo, on the other hand, conserve the whole sedimentary sequence and are largely surfaced by UCL at a relatively high elevation, underlain by the BC layer, except for eroded topographical features.

As mentioned in Section 2, in this study we performed ambient noise measurements; these were used to investigate the dynamic characteristics of features at different stages of the destabilization process affecting the cliff area on the Maltese Islands. In fact, the archipelago has several areas of coastal instability characterized by active lateral spreading, rock sliding and rock falls. The instability happens to be situated in areas of coastal land that are used as amusement parks [10], urban areas [11], as well as cultural heritage sites; it has therefore solicited some concern.

In the northern part of the island of Malta, as well as in Gozo, the geomorphology is mostly dictated by the fact that the UCL forms a rigid rock slab resting on a much weaker layer of clayey material. This geological situation creates stresses in the upper slab resulting in fracturing and brittle collapse [12]. When the exposure of the geological cross-section is along the coast, the additional weathering effect of marine processes accelerates the destabilization by erosion of the clay layer. This results in the formation of large cliff-parallel surface fractures that produce partially isolated blocks having volumes of the order of thousands of cubic metres. Horizontal and vertical mass movement of such blocks forming part of the cliff face, and boulder detachment and collapse, result in a fractured and boulder-strewn coastline, that is typical of much of the northwest coast of Malta.

## **4. RESULTS AND INTERPRETATION**

### **4.1. MEASUREMENTS IN THE GOLDEN BAY**

We performed a first set of measurements in the Golden Bay area, in the vicinity of Ghajn Tuffieha Tower. The tower is part of the fortification



structures built by the knights of St. John. In particular, it belongs to the “Lascari towers” constructed between 1637 and 1652 and commissioned by the Italian knight Giovanni Paolo Lascaris who was Grand Master of the Order. The area is affected by the presence of later spreading and retreating of the cliff edge, due to the fracturing of the Upper Coralline overlaying the Blue Clay, as explained in Section 3.

The area prospected with GPR is approximately indicated by a red rectangle on the Google satellite map reported in Figure 2. This area was chosen because of the presence of large fractures in the nearby region. The arrows show two points where the soil collapsed. Figure 2 also shows the location of the single-station measurements and the position where H/V results were obtained, whereas Figure 3 presents the passive-seismic results.

By examining Figure 3, notable characteristics can be identified for each investigated location. The first important observation is the presence of an ubiquitous resonance peak between 1.0 Hz and 2.0 Hz, and a dip in the spectral ratio below 1.0 over a wide frequency range. This is not surprising because previous ambient noise studies did repeatedly confirm similar results [11, 13, 14]. The dip in the H/V ratio can be interpreted in terms of a shallow shear-wave velocity inversion, which in this case corresponds to the interface between the UCL and BC. The interpretation of other features of this peak, in terms of Rayleigh wave ellipticity and/or trapping of SH waves in the low-velocity layer, is the subject of an ongoing study that makes use of numerical modelling. Moving from the inland area towards the cliff edge and rock sliding area, the nature of the H/V response changes strikingly. On the plateau away from the cliff edge, the site response shows only the simple and consistent peak at around 1.5 Hz, as described above, whereas the rest of the H/V amplitudes remain at a level well below 2.0. Moreover, it is noted that at higher frequencies of the spectrum there are peaks not observed on the plateau area, which may be tentatively associated with mechanical vibration modes of the whole blocks.

The area investigated by using the GPR is about 5.2 m × 6.5 m wide. This area was prospected by acquiring a series of parallel B-Scans, directed toward the sea and spaced 40 cm from each other. All the B-Scans end in proximity of the cliff, which is about 30 m high and sharply overhanging the sea.

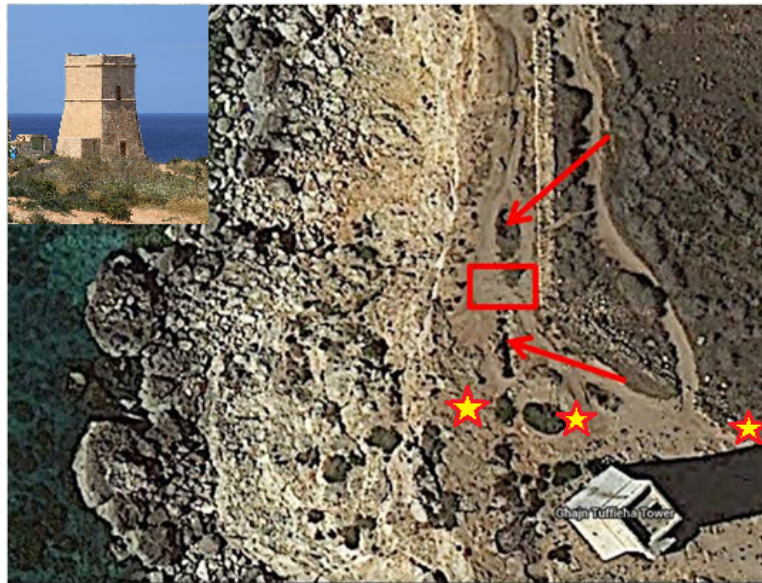


**FIG. 2** – Golden Bay. The area prospected with GPR is approximately indicated by a rectangle. The arrows show two points where the soil is collapsed. The stars indicate the location of single-station measurements.

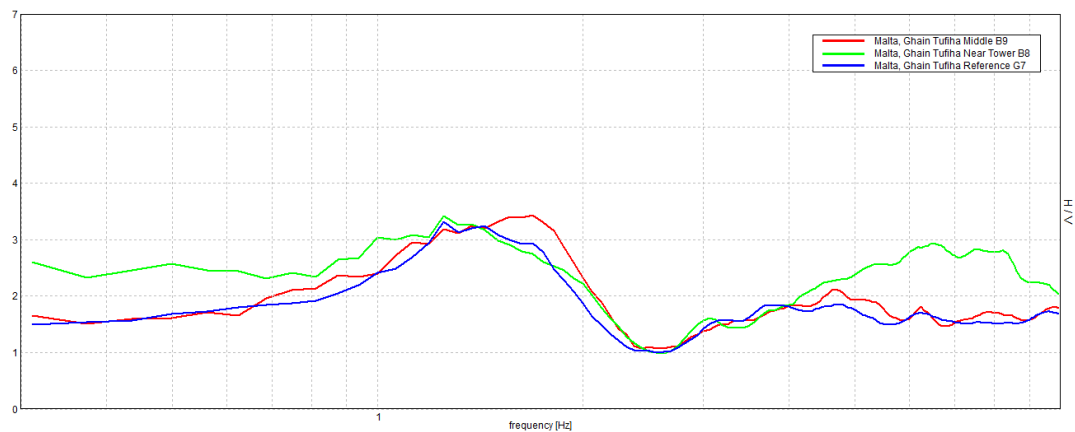


**FIG. 3** – H/V curves (average H/V versus frequency) obtained at the three different sites, in the Golden Bay.

In Figures 4-7, horizontal slices at different time-depth levels are reported, showing that the subsidences have a deep track. The two subsidences appear to be separated; however, they could join each other in the future, if the phenomenon is progressive. In this case study, the data recorded by the low-frequency antennas have been exploited, because the anomalies of interest are quite extended and it was important to achieve a high penetration depth of the signal. The

data processing was minimal and included zero timing, application of gain versus depth, background removal, and slicing [15]; no migration was performed, being the anomalies quite large; the Reflexw commercial software was used [16]. Let us mention that the conversion time-depth was done on the basis of the fact that the cliff is made of limestone and the soil was dry. The B-Scan did not show any meaningful hyperbola associable to a small target, therefore the method of the diffraction hyperbolas [17, 18] was not applicable, neither we had at disposal separable antennas in order to perform a common mid-point (CMP) measurement.



**FIG. 4** – Horizontal slice at shallow depth, superimposed on the Google satellite image of the Golden Bay.



**FIG. 5** – Horizontal slice at 15 ns, corresponding to a depth of about 85 cm.

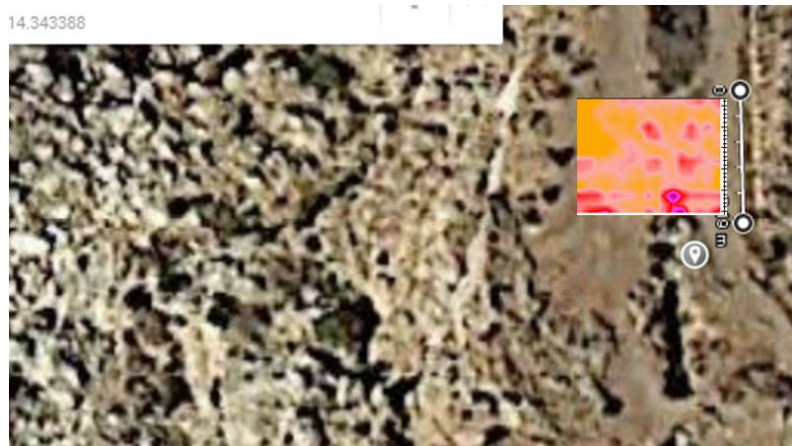


**FIG. 6** – Horizontal slice at 30 ns, corresponding to a depth of about 170 cm.



**FIG. 7** – Horizontal slice at 50 ns, corresponding to a depth of about 280 cm.

#### 4.2. MEASUREMENTS AT LAFERLA CROSS, MALTA

After the case study of the Golden Bay, essentially done for geological reasons, we dealt with a survey of interest for both geological and engineering reasons, which also reminded us of a previous study carried out in Italy [19].

The church of Laferla is an abandoned construction on the top of a small hill, near to Laferla Cross. In Figure 8, the church is the building on the low-middle part of the image. There is a geological sliding in that area, which has strongly damaged the church. Indeed, the access to the church is prohibited because dangerous. People living in the area are attached to this old church and there are proposals of moving the

building away from its current position. We performed a preventive investigation, to check the situation of an area nearby the church.

It was not easy to perform a complete series of parallel B-Scans here, because of the irregular topography of the soil, and so we performed 6 B-Scans, as referenced in Figure 8. We did not have at our disposal a GPS system; therefore, the position of the B-Scans is qualitative, based on our sketches and on some distances taken by us in the field. Due to the purposes of this prospecting, the most interesting data were those recorded by the medium-frequency antennas. The processing was the same as that described for the Golden Bay, but the data have been migrated too, because in this case it was possible to evaluate the propagation velocity from diffraction hyperbolas (the estimated value was about 12 cm/ns). In the following, we discuss and interpret the various B-Scans.

In Figure 9, the processed B-Scan No. 1 is shown. This B-Scan was recorded parallel to one of the sidewalls of the church, which has a big fracture in its central part. We were therefore looking for something buried in the subsoil, which could be correlated to this fracture. The B-Scan shows some anomalies, the most evident of which is at the abscissa 80 cm and between 10 ns and 20 ns: we deem it ascribable to some boulder or ashlar (because it is large, but the reflection is not strong), and not to the fracture.

The processed B-Scan No. 2 is presented in Figure 10. Here, we appreciate that the soil is layered in the first 20 ns (corresponding to about 120 cm) and we also see at least three relevant discontinuities. The strongest one, between the abscissas 8 m and 10 m, is possibly related to a cavity with reinforced ceiling. In fact, it is known that there is a cavity in that area, which ceiling was reinforced; maybe, the floor of the cavity produces the multiple flat reflections that can be seen below that anomaly. Another strong but localized anomaly is visible around the abscissa 5 m: this might be associated to some boulder. Two further meaningful discontinuities can be observed under the first 2 m of the scan, between the abscissas 16 m and 18 m. The second one of these discontinuities is quite meaningful and might be related to another cavity, else to a part of the same cavity visible between the abscissas 8 m and 10 m, but with a non-reinforced ceiling. There is also an anomaly visible in the first meters of the B-Scan, possibly connected to the B-scan No. 6 as discussed later on.



**FIG. 8** – La Ferla church and the B-Scans performed close to it.

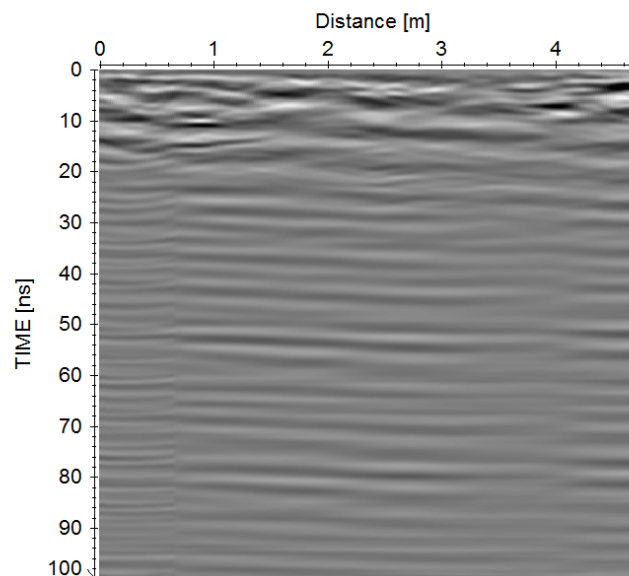


**FIG. 9** – B-Scan No. 1 of Fig. 6.

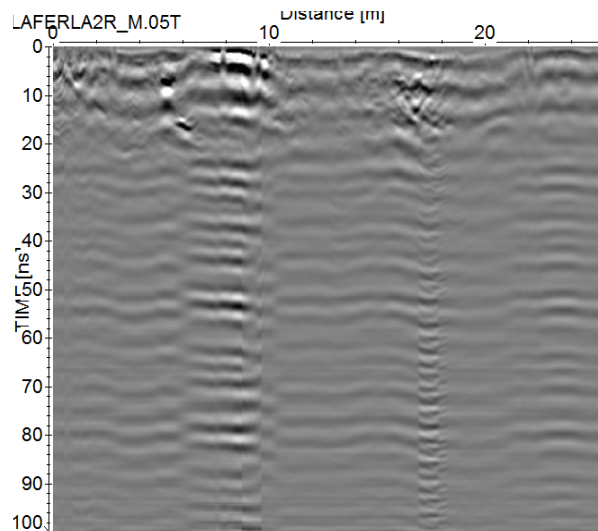


**FIG. 10** – B-Scan No. 2 of Fig. 6.

The processed B-Scan No. 3 is reported for the sake of completeness in Figure 11, but these data do not show any anomaly of interest apart from a confirmation of some layering of the shallower part of the soil.

The processed B-Scan No. 4 is presented in Figure 12 and shows a large anomaly between the abscissas 2 m and 6 m. This anomaly is probably related to the one visible in B-Scan No. 2 between the abscissas 16 m and 18 m, and it enforces the hypothesis of a buried cavity in that area. A second anomaly is present in B-Scan No. 4, between the abscissas 8 m and 12 m. This anomaly seems to be the contact line between two zones with different properties of the soil and might be related to some work done in the past.

The processed B-Scan No. 5 is reported in Figure 13. Here, we see a strong and large superficial anomaly between the abscissas 5.2 m and 8 m, which we ascribe to the reinforced ceiling of a cavity. In particular, we deem that this strong anomaly can be related to the strong superficial anomaly visible between 8 m and 10 m in B-Scan No. 2. A meaningful reflection among the abscissas 10 m and 12 m is also visible in Figure 13, possibly ascribable to a material of different consistency.

Finally, in Figure 14 the processed B-Scan No. 6 is presented, where several anomalies are visible. We identify an oblique descending part of the trace in the first part and an oblique ascending part from about 6 m and 8 m. We know that in that area a collapse happened in the past

and was filled up. We interpret the B-Scan No. as a cut of the collapsed area. In particular, looking at the displacement of the B-Scans and at the first 7.5 m of B-Scan No. 2, we notice some resemblance between the sort of filled tank that appears in B-Scan No. 6 and something similar in B-Scan No. 2, indicating possibly two different cuts of the same collapsed and subsequently filled up hole.

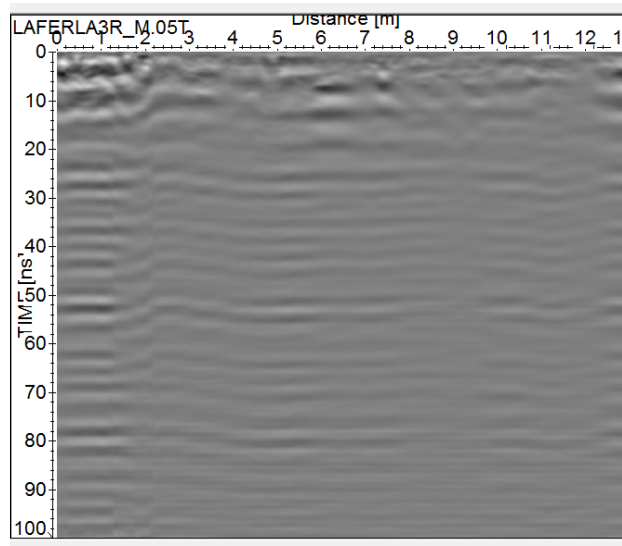


**FIG. 11** – B-Scan No. 3 of Fig. 6.

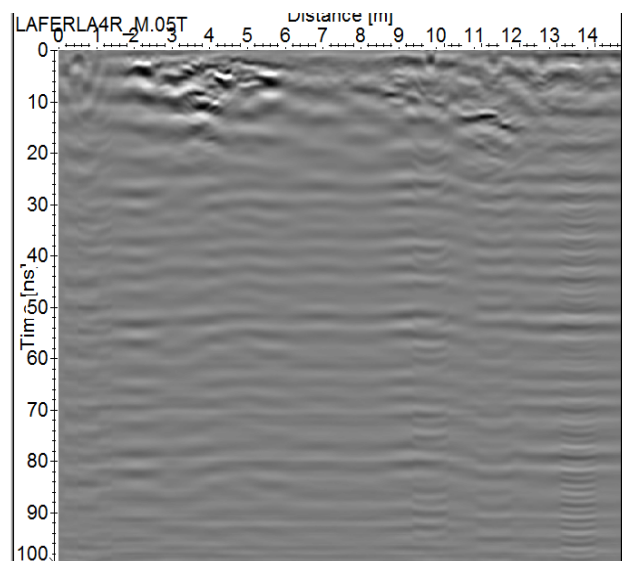


**FIG. 12** – B-Scan No. 4 of Fig. 6.



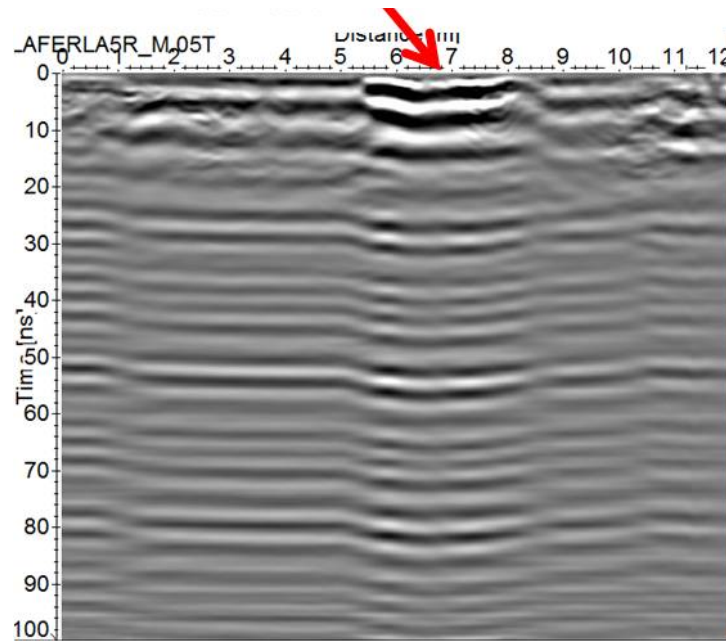


**FIG. 13** – B-Scan No. 5 of Fig. 6.

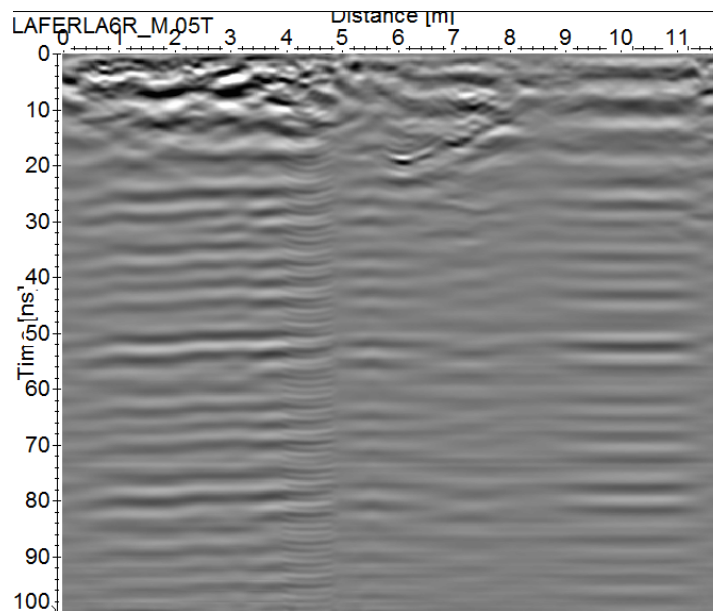


**FIG. 14** – B-Scan No. 6 of Fig. 6.

Overall, the GPR measurements show a stratified soil, at least in the shallower layers (down to about 1.2 m), with several anomalies, part of which may be ascribable to buried cavities.

### 4.3. MEASUREMENTS IN MADLIENA TOWER, PEMBROKE

Madliena tower is a mighty structure, exploited as a watchtower between 1658 and 1659; it has with very thick walls, because it was a military defensive structure. A photo of the tower is shown in Figure 15.

The inner of the tower, at the ground floor, is a rectangular room with size 2.9 m × 3.9 m, plus a small corridor towards the entrance door. We prospected the room by using our GPR prototype, with spacing between parallel profiles of 20 cm. We exploited an option of the instrument that allows assembling the manhole in a vertical position. Usually the manhole of a GPR is slightly oblique, because in this way the human strength for pushing the instrument is dynamically better exploited. However, an oblique manhole is practical (and in many cases essential) when the prospecting is done on the grass. Indoor, the mechanical resistance to the rotation of the wheels is customarily much lower, and a vertical manhole allows saving space and prospecting a larger area.



**FIG. 15** – Madliena tower at Pembroke.

In Figures 16-19, depth slices at different depths are shown. These data were gathered with the medium-frequency antennas and the processing steps were the same as in the investigations presented in the previous subsections of this paper. In the present case study, the data were not migrated because we did not have accurate information about the propagation velocity. The GPR results suggest the presence of a

foundation structure, with walls reaching a depth of at least 1 m in the subsurface, possibly enlarging with depth. Such foundation is probably excavated directly in the rock. The lack of an accurate value of the propagation velocity prevents us from more detailed evaluations.

The tower was also probed with a passive seismographic device: the results are presented in Figure 20. Measurements were taken at the top and middle levels of the tower, and at the ground floor. The ground-floor data confirm that the tower is located on a solid rock: as seen in previous studies, this gives a flat response in the H/V curve [13, 14]. The high-frequency peaks (between 100 Hz and 200 Hz) may be due to a thin layer of soil (shown also by the GPR), but further investigations and numerical modelling are needed to confirm this hypothesis. At the roof level, the fundamental frequency (i.e., the lowest frequency of the building) is clearly identified at about 6 Hz. Higher frequency modes were difficult to identify because the structure is not very high.

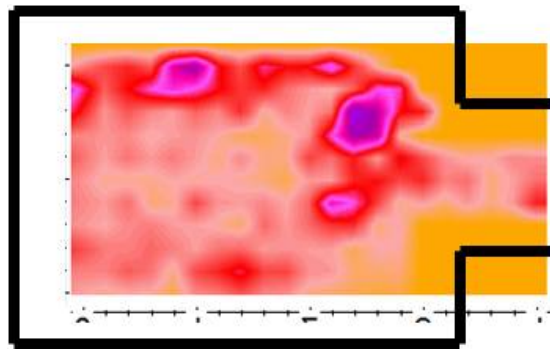


**FIG. 16** – Horizontal slice at 5 ns (about 25-35 cm), from data recorded at the ground floor of Madliena tower. The homogeneous orange colour indicates areas where the GPR instrument could not pass.

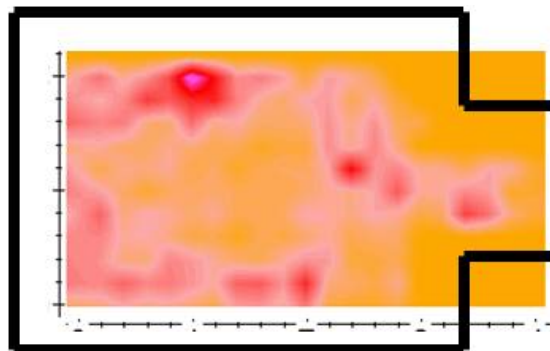


**FIG. 17** – Same as in Fig. 16, at 10 ns (about 50-75 cm).

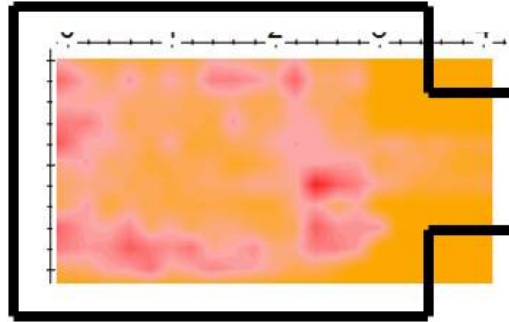


**FIG. 18** – Same as in Fig. 16, at 15 ns (about 75-108 cm).

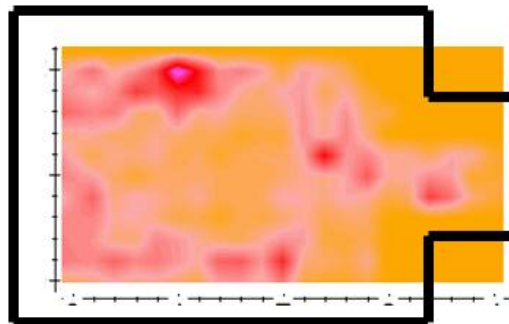


**FIG. 19** – Same as in Fig. 16, at 20 ns, about (100-150 cm).

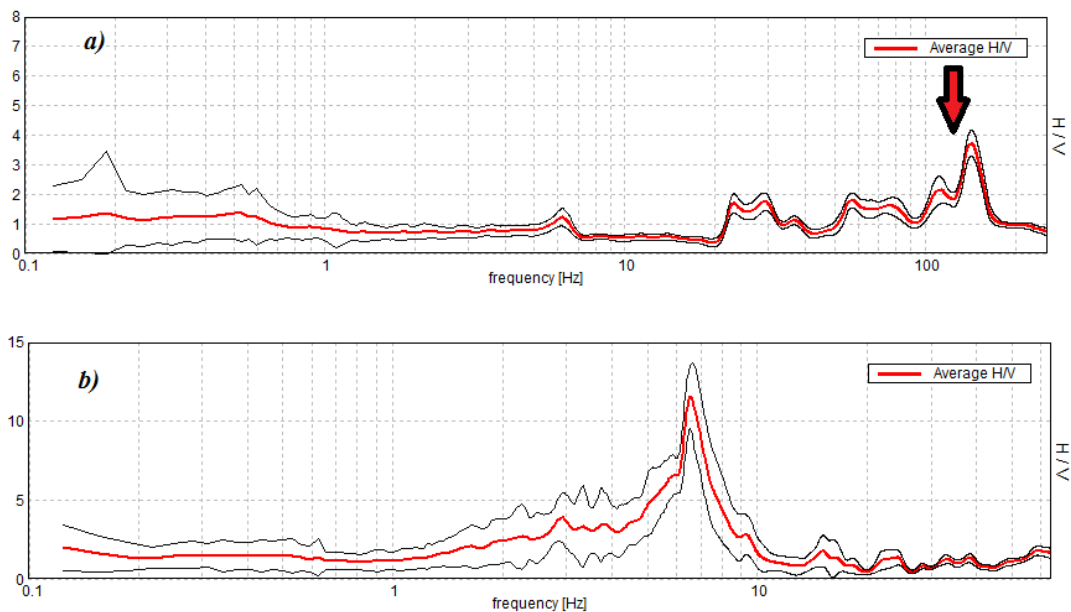


**FIG. 20** – Seismographic results in Madliena tower. The top and bottom panels show results obtained on the ground floor and at the roof level, respectively.

#### 4.4. MEASUREMENTS OUTSIDE THE CHURCH OF SANTA MARIA, BIRKIKARA

Measurements were performed also outside the church of Santa Maria, a historical building where structural problems had been noticed. In particular, some fractures and movements of the walls were observed.

GPR data were gathered with 50-cm spacing between adjacent profiles. The results presented in Figure 21 (horizontal slices at different depths) were recorded by the medium-frequency antennas. The processing was the same as in the previous cases. The notch on the white lines corresponds to a length of 2 m. The homogeneous orange colour indicates areas where the GPR could not pass.

The data show a confused situation at the shallowest levels, which were strongly reshuffled in the 20th century. After 10 ns, more isolated

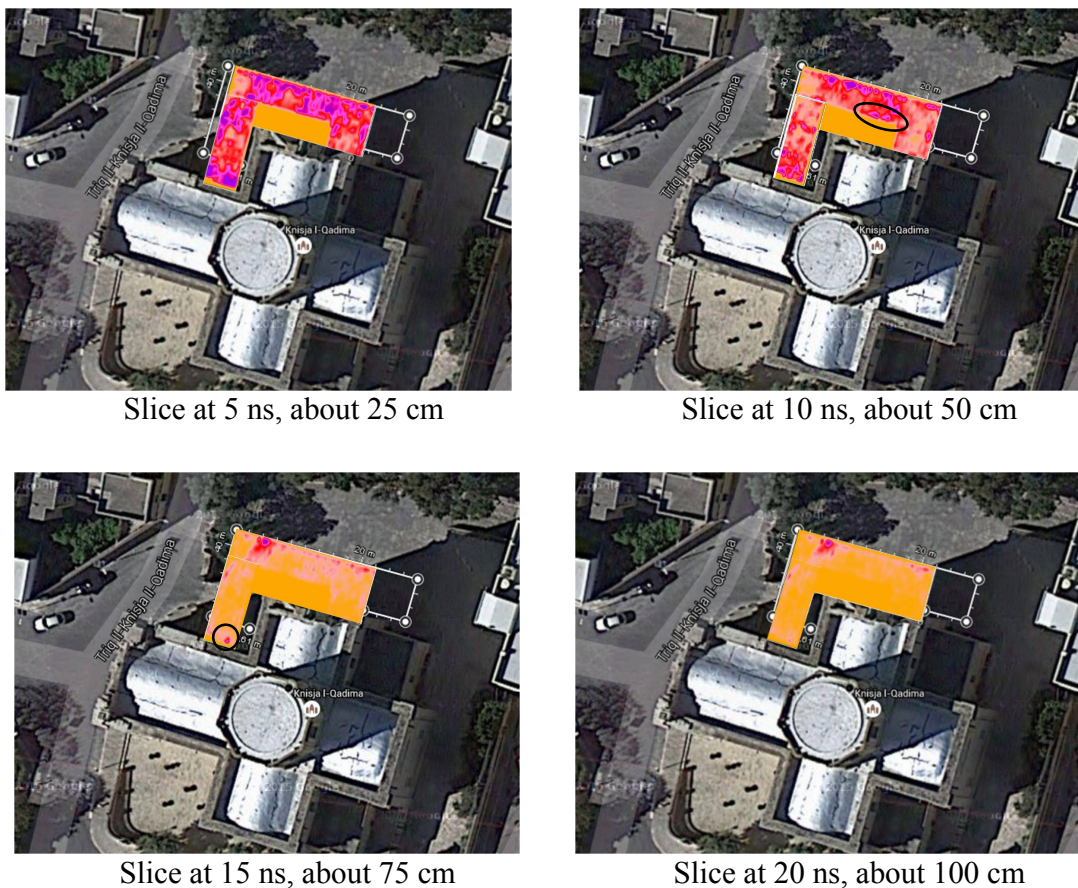


**FIG. 21** – Horizontal slices at different depths outside the church of Santa Maria.

anomalies are visible. The anomalies farthest from the wall of the church are at least partially ascribable to tombs; indeed, it is known that there was a cemetery in that area. Some clear anomalies close to the walls of the church are outlined by the ellipsis superimposed to the slice at 10 ns and by the circle superimposed to the slice at 15 ns; they might be related to the structural problems that the building is having.

Three B-Scans were recorded along the sidewalk that runs around the church structure, in order to gather some data very close to the building. The location of the B-Scans is shown in Figure 22, whereas the results are shown in Figure 23. Looking at Figure 23, we see in B-Scan No. 1 a rather clear discontinuity, suggesting the presence of a two-layered soil in the first part of the profile. The time depth of this interface oscillates slowly around 15 ns (about 75 cm). Several stronger reflections are present in B-Scan No. 1, indicating maybe past works with heterogeneous materials used for the filling. Overall, the prospecting reveals clearly that the most inhomogeneous conformation is under the line of B-Scan No. 1.

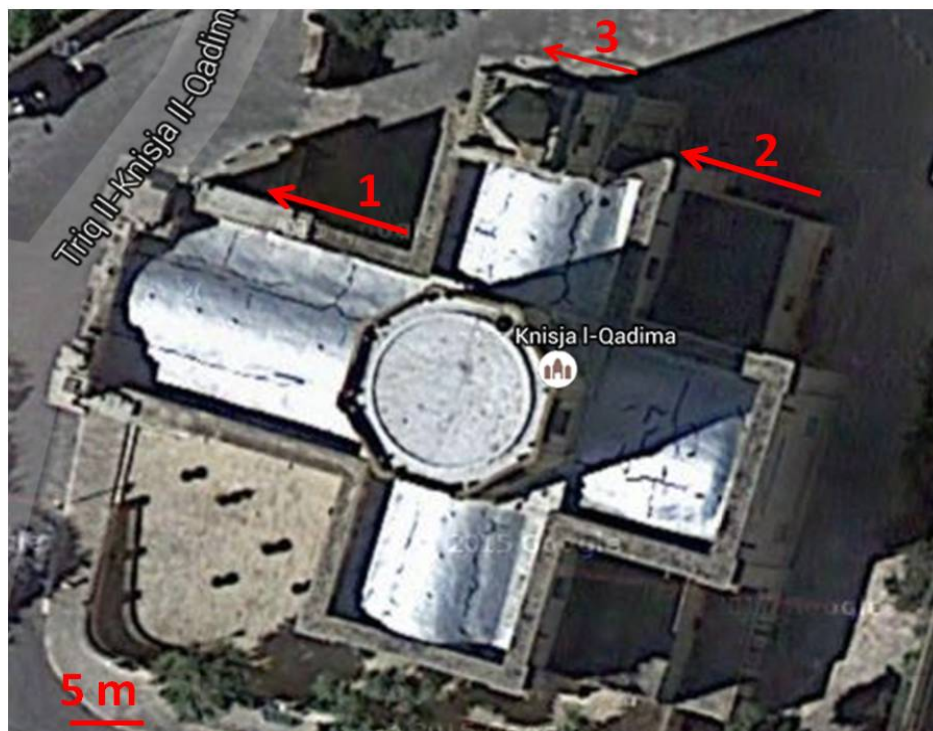


**FIG. 22** – The displacement of three B-Scans gathered around the church of Santa Maria.

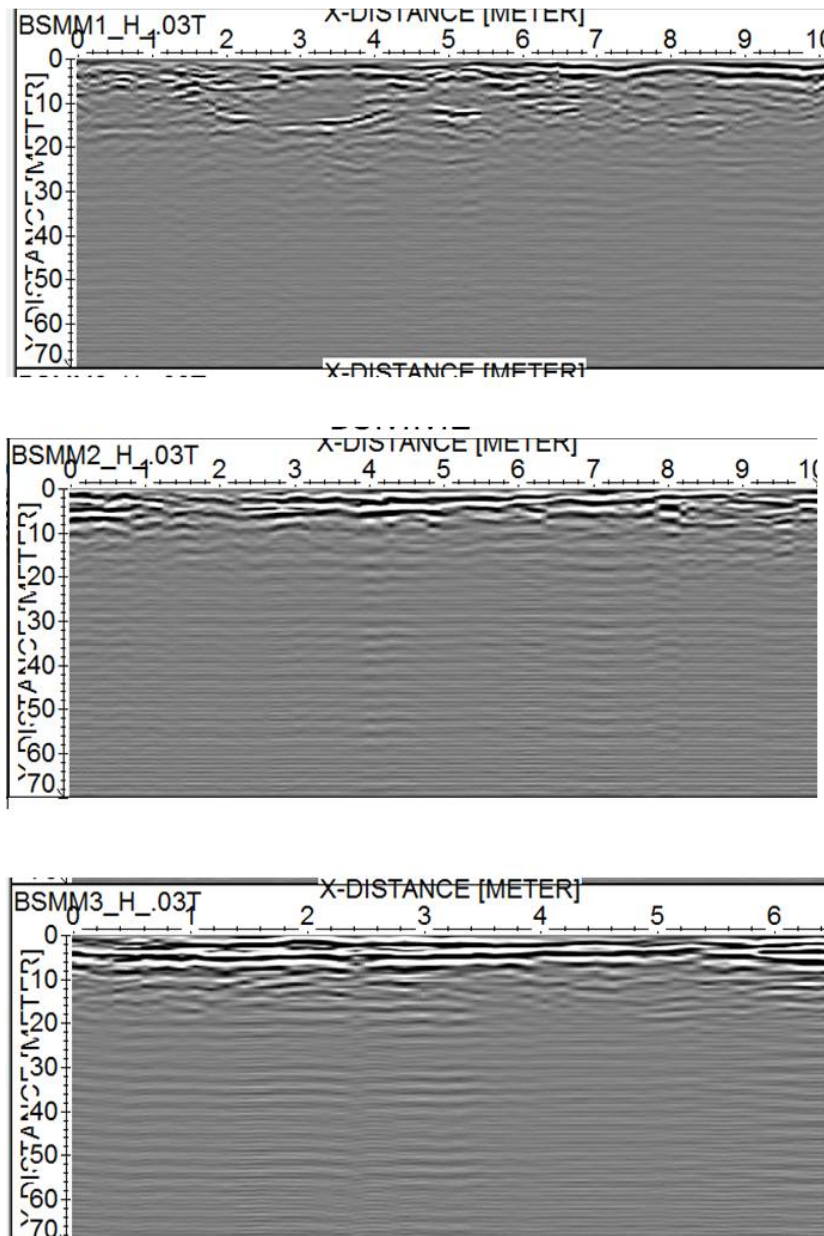


**FIG. 23** – From top to bottom, the processed B-Scans No. 1, 2 and 3 as indicated in Fig. 17.

#### 4.5. MEASUREMENTS IN THE CO-CATHEDRAL OF ST. JOHN, LA VALLETTA

Measurements were performed in the co-cathedral of St. John, which is an important monument, patrimony of UNESCO, with precious frescoes and paintings, as well as the tombs of many knights of the order of Malta, including some Grand Masters of the knights. Both GPR and passive

seismographic data were gathered in the co-cathedral. The obtained results are presented in this subsection of the paper.

With regard to the GPR data, a small rectangle evidenced in Figure 24 was prospected with interline spacing of 40 cm. Moreover, three B-Scans were recorded in the main nave, as shown in Figure 24.

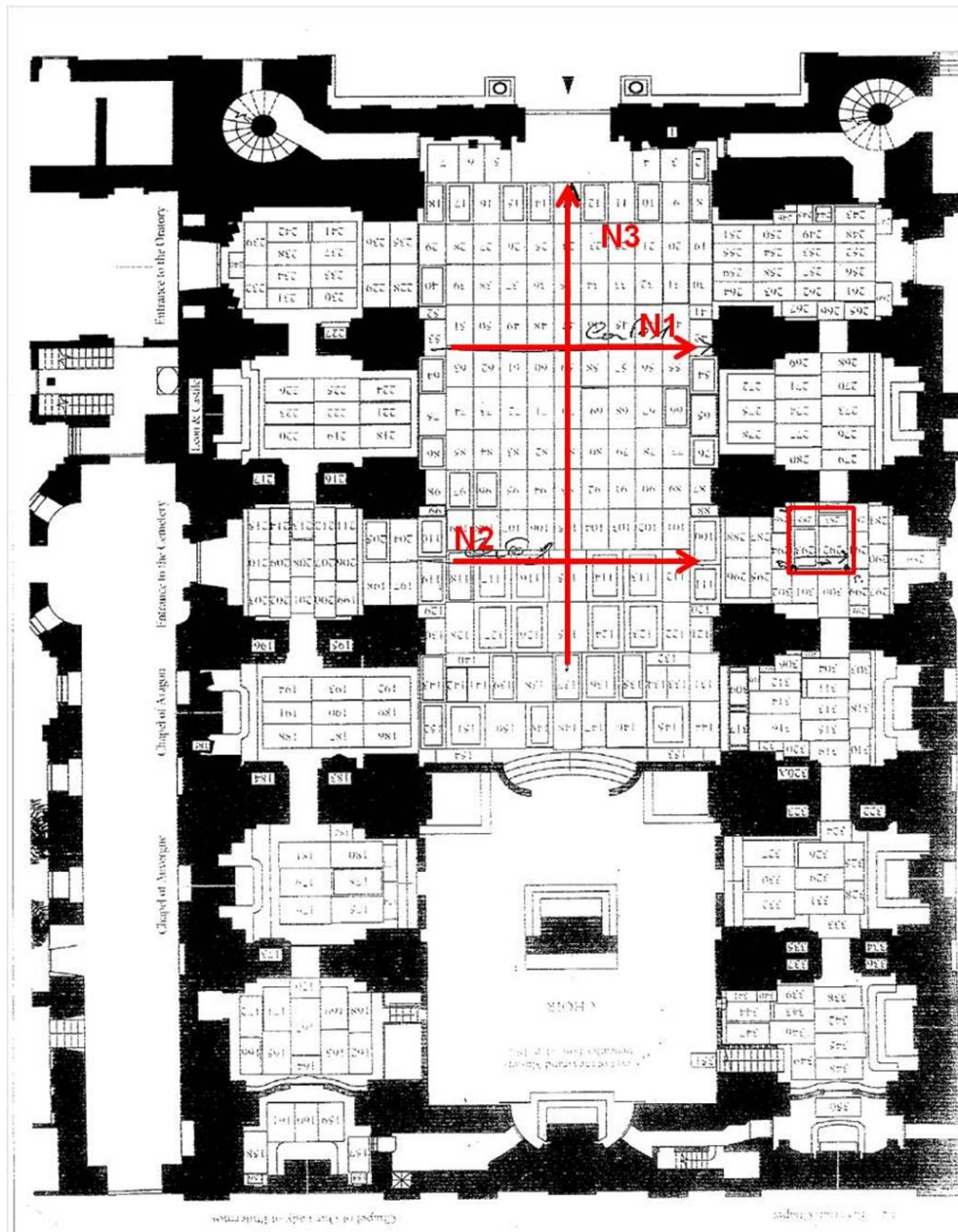


**FIG. 24** – Map of the GPR prospecting in the co-cathedral of St. John.



The data gathered on the rectangle in the lateral chapel (where nowadays is the entrance for the tourists) were aimed to establish whether a crack on a gravestone on the floor is due to a void under it. In fact, the floor of the church is a sequence of gravestones, but not all of them really correspond to an underlying tomb. GPR data were therefore recorded on a small rectangle (2.4 m × 3.1 m) approximately centred on the crack. This time, the high frequency antennas were exploited, as the crack was likely to be related to a possible cause buried in the first meter at most. The obtained results are reported in Figure 25 and reveal the presence of superficial inhomogeneous features, no meaningful cavities are seen. This suggests that the causes of the crack must be superficial.

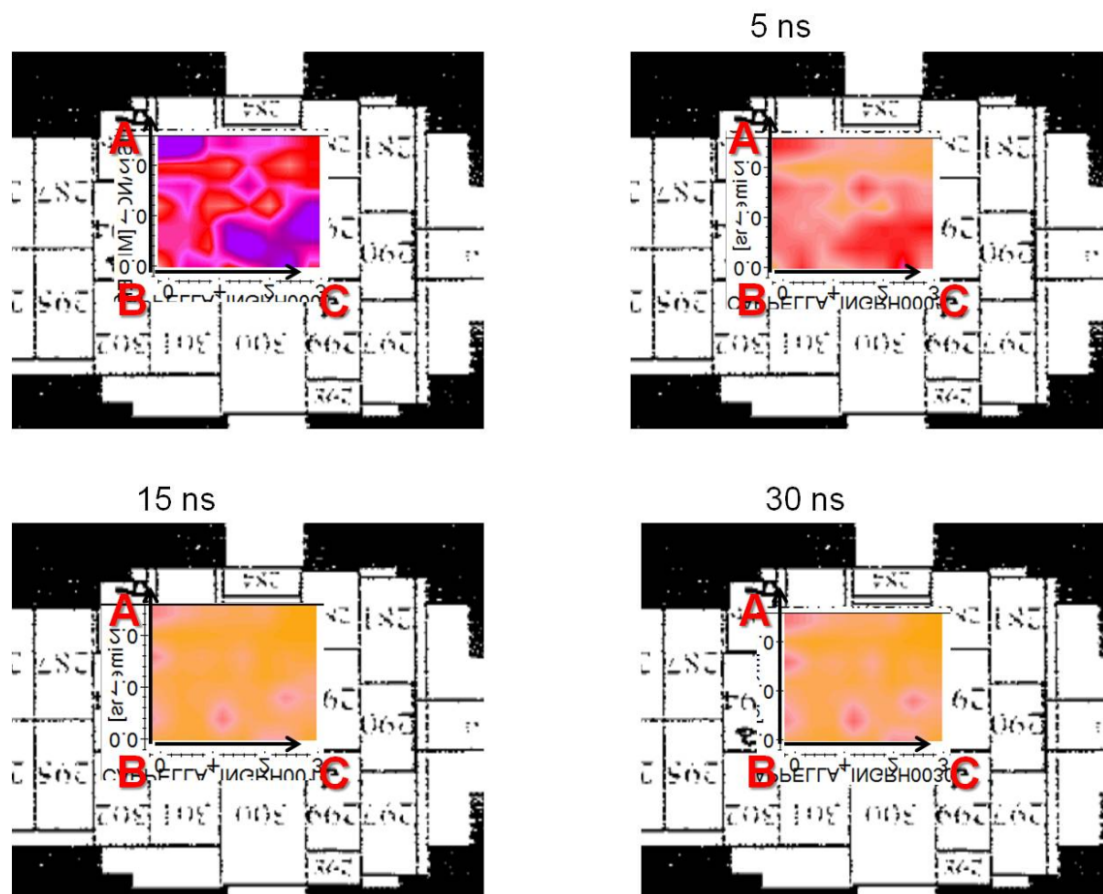


**FIG. 25** – Horizontal slices in the entrance chapel of the co-cathedral of St. John. For time depth conversion: the upper left slice is quite superficial (about 5 cm - 7 cm), 5 ns correspond to about 25 cm, 15 ns correspond to about 75 cm, and 30 ns correspond to about 150 cm.

When present, shallow cavities are usually well visible, as can be appreciated from the results recorded in the nave of the church and presented in Figure 26. In general, single B-Scans are not sufficient to foresee the presence and position of tombs (horizontal slices are well advised for that). However, in the case at hand the presence of tombs is revealed in the areas where several multiple reflections occur: such reflections are well visible in several points of the B-Scans, and are particularly evident in the longitudinal B-scan No. 3, probably because this one crosses some tombs along their long side.

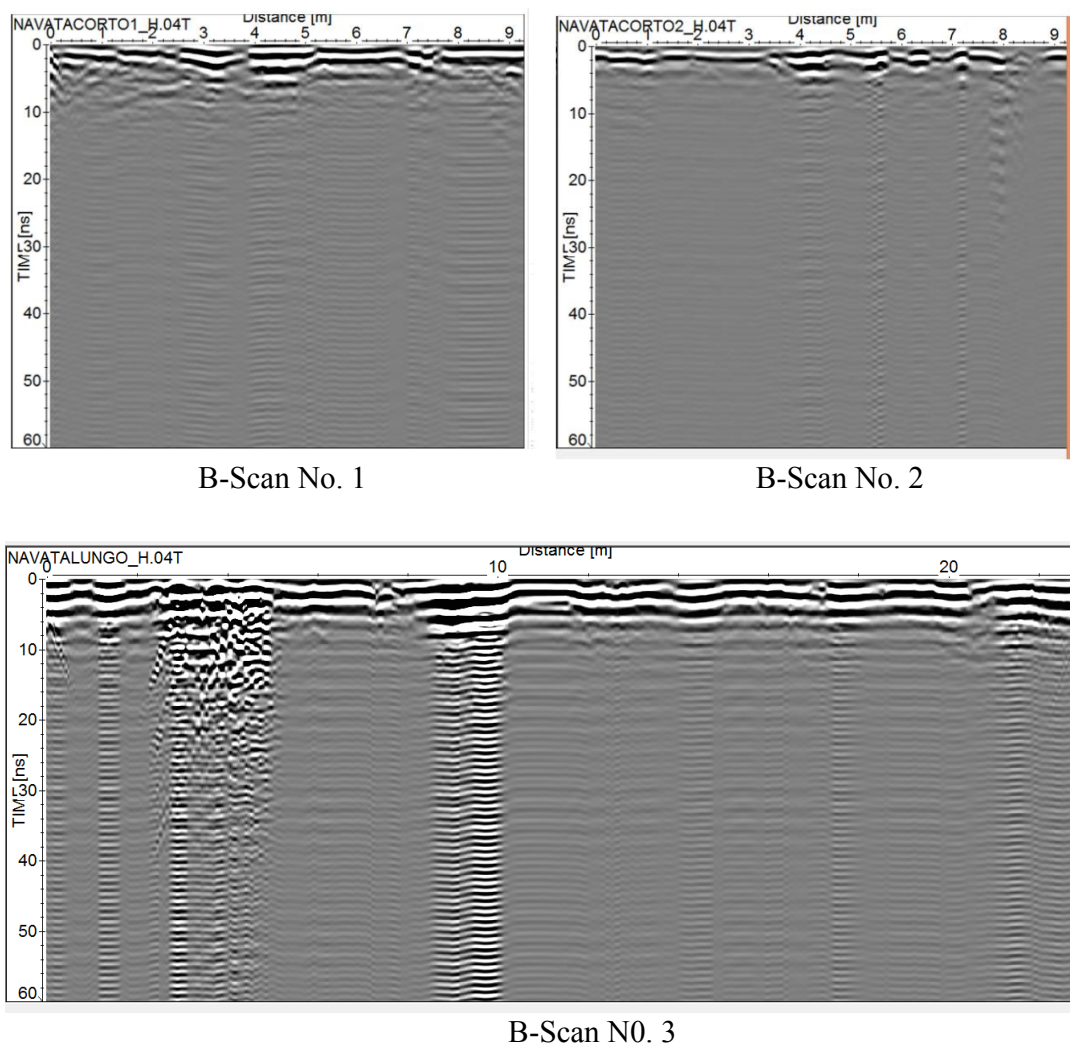


**FIG. 26** – B-Scans gathered in the main nave of the co-cathedral of St John.

#### 4.6. TESTING THE RECONFIGURATION OF INTEGRATION TIMES

As mentioned in Section 2, the stepped-frequency GPR prototype allows gathering data with three couples of antennas and reconfiguring the integration times of the transmitted and received harmonic tones.

In the framework of the investigations presented in this paper, in some cases the most useful data were recorded by the low-frequency antennas (e.g., at Golden Bay), in some other cases the most interesting data were gathered by the medium-frequency antennas (e.g., Laferla Cross, Madliena tower, Santa Maria church), and we exploited the high-frequency data for the study carried out in the co-cathedral of St. John. Our system gathered three sets of data in each site, and so, for further possible analyses, we have at our disposal other data, beyond those reported and interpreted in the previous sub-sections of the paper.

The reconfiguration of the integration times was performed everywhere, apart for Golden Bay, due to technical problems that could be solved only after that (first) prospecting. So, the data of Laferla cross, Madliena tower, Santa Maria church and St. John co-cathedral have been gathered after a reconfiguration of the integration times. We will show here how the system is able to recognize the interferences, according to the algorithm described in Section 2, and how the data look slightly cleaner – in a couple of cases – after the reconfiguration of the integration times. The effects of the interferences are not strong in the cases at hand, both because there was no strong source of interference close to the investigated areas, and because the prototype uses default integration times quite longer than those of commercial systems.

In Figure 27 we show the variance of the tones (see Section 2) for data recorded at Laferla Cross and Madliena tower. As can be noticed, in both cases the most disturbed frequencies are in the lower part of the 50–1000 MHz range. This happens most times, first of all because FM broadcast transmissions usually occupy the band around 100 MHz, and also because the GPR antenna shielding is customarily less efficient at low frequency. We observe that the variance level measured at Laferla cross is much higher (3 orders of magnitude) than that gathered inside Madliena tower. This is coherent with the fact that Madliena tower is a historical building with rather thick walls, which isolate the internal room from the external environment, whereas Laferla Cross is an outdoor site.

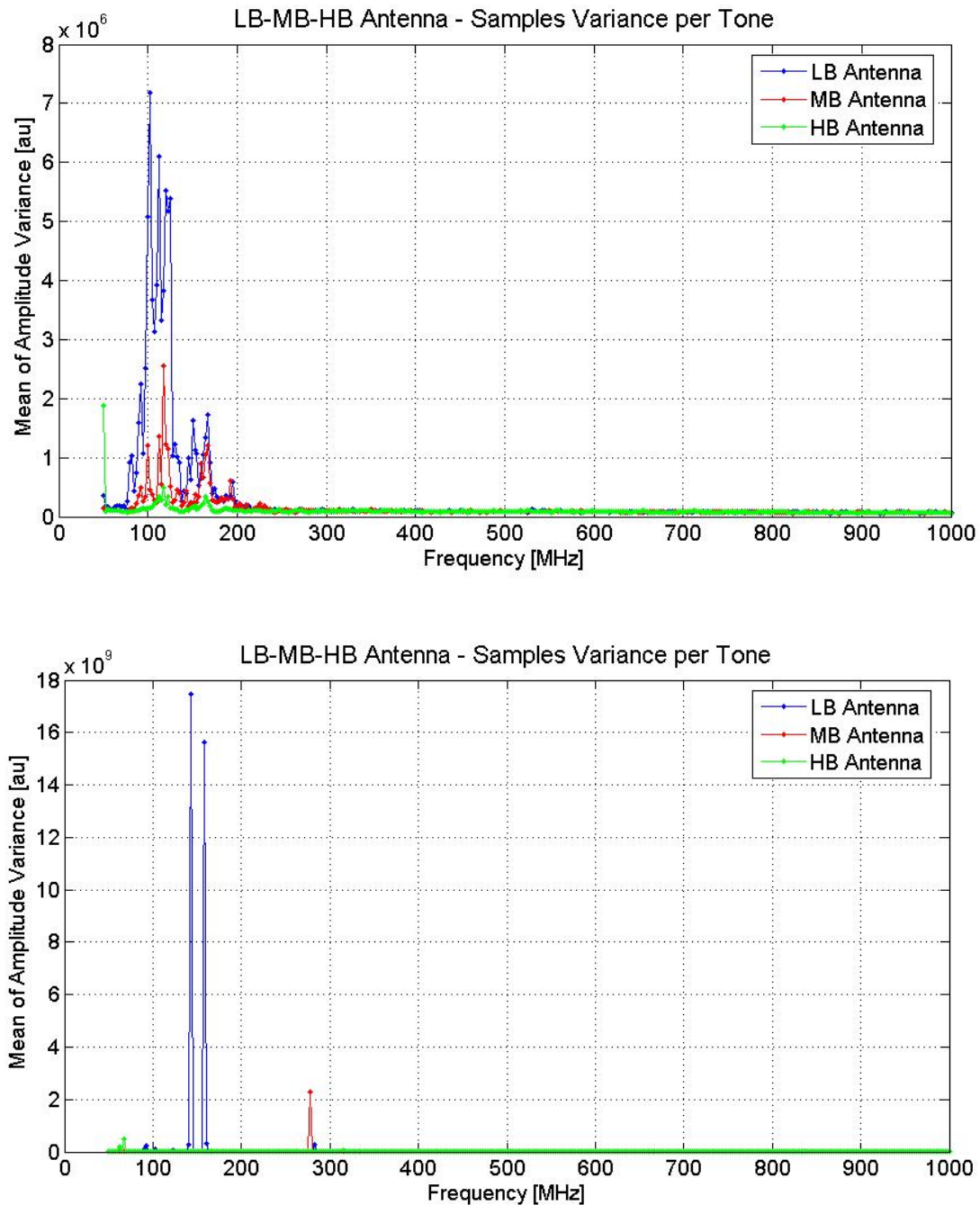


**FIG. 27** – The variance of the tones in the site of Laferla Cross (upper panel) and in the site of the Madliena tower (lower panel).

In Figure 28, the variance of tones for two scans gathered outside the church of Santa Maria is shown. We recorded two calibration B-Scans to check whether the graph of the variance of the tones was strongly

dependent on the position of the B-Scan; the two B-Scans were at about 20 m of distance from each other and not parallel to each other, moreover they were on two different sides of the building. As can be seen, the results are not the same, and indeed the level of the disturbance changes of one order of magnitude, but the most disturbed frequencies are the same. In particular, in both cases there is a peak around 100 MHz and another one around 200 MHz. We were then informed that there is a radio station near the church, transmitting with a carrier of 99 MHz, which explains the peaks. Apart from this, the measurements prove the reliability of the method, because the most disturbed frequencies are essentially related to the area and not to the particular B-Scan.

In Figure 29, the variance of the tones recorded in the co-cathedral of St. John is shown. We first measured the variance shown in the upper panel of the figure; then, we saw the transceiver devices used by the staff of the co-cathedral (which nowadays is also a museum) and we gathered a second calibration, along the same measurement line and after switching on a transceiver. The carrier of the transceiver is at 446 MHz, and coherently, a localized disturbance is visible at this frequency in the lower panel of Figure 29. We can see that the disturbance due to the transceiver is at a much higher level than the previously recorded one, which was, instead, of the same level as the disturbance recorded in the Madliena tower (also in this case, in fact, we were indoor, in a historical building with thick and partially isolating walls). We decided to calibrate the reconfiguration of the GPR on the basis of the possible interferences from the transceivers. In the previous case studies, we set  $F = 10$  for the low and the medium frequency antennas in the sites of Laferla, Madliena tower and Santa Maria church, and we used  $F = 1$  for the high frequency antennas in those cases. In the co-cathedral, instead, we set  $F = 10$  for all the antennas. The prolongation factor of the integration time for each tone is shown in Figure 30.

In Figure 31, the same observation line was walked through two times, without and with reconfiguration, in the site of Laferla. Analogous results are shown in Figure 32 for the site of Madliena tower and in Figure 33 for the site of Santa Maria church. Finally, the same comparison was performed in the co-cathedral of St. John and relevant results are presented in Figure 34. We notice some effects of the reconfiguration in the sites of Laferla and St. John, whereas in the sites

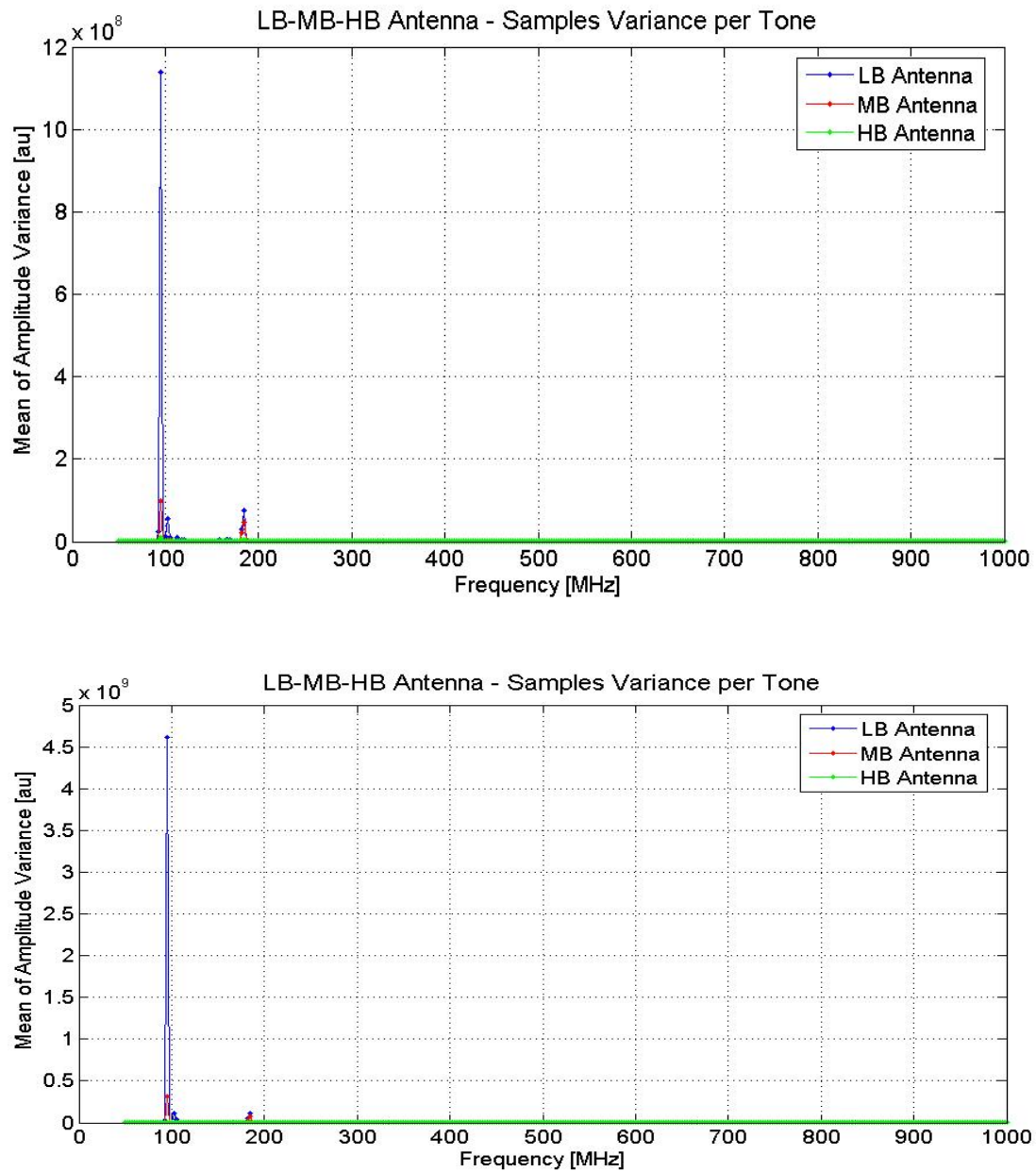


**FIG. 28** – Variance of the tones measured along two B-Scans outside the church of Santa Maria.

of Santa Maria and Madliena Tower, the effects are not appreciable on the shown scale. With regard to the site of Madliena tower, this is easily understood because of the isolating walls. Outside Santa Maria church, there was a stronger interference than inside Madilena tower, but this mostly regarded the low frequency antennas, whereas we are now

analysing at medium-frequency antenna results. In particular, if we have another look at the curves shown in Figures 27 and 28, we can appreciate that the level of interference was in any case weaker at Santa Maria church than at Laferla, and also that the level of interference at Santa Maria church was stronger for the low-frequency antennas, whereas the variance of the tones of the medium-frequency antennas has an appreciable peak at about 290 MHz in the site of Laferla.

## 5. CONCLUSIONS

In this report we have presented the main results achieved during the Short-Term Scientific Mission (STMS) entitled “Use of GPR and standard geophysical methods to explore the subsurface,” funded by COST Action TU1208. We performed measurements in various sites of geological and/or cultural interest in the island of Malta.

Integrated Ground Penetrating Radar (GPR) and passive seismic surveys were carried out. The reconfiguration of the integration times of the harmonic components, an advanced feature recently implemented in a stepped-frequency GPR prototype, was tested on field data. With regard to this last point, the work is in progress and further tests will be done in the future to optimize and thoroughly characterize the performance of the system and the effectiveness of the reconfiguration of the integration times.

Let us underline that the reconfiguration of the integration times is a totally new feature of our GPR system. The algorithm for setting the reconfiguration on the basis of data gathered in the field is specifically related to an upgrade of the system, which was possible thanks to previous studies performed during the STMS carried out by Dr. Loredana Matera in Trondheim (Norway) in June 2014 [2]. That STSM was also funded by COST Action TU1208 and was hosted at the headquarters of 3d-radar, a well-known manufacturer of commercial stepped frequency systems.

We also wish to mention that the fruitful cooperation between IBAM-CNR and the University of Malta started thanks to the COST Action TU1208, with the STSM presented in this paper. We subsequently had the opportunity to strengthen our cooperation by organizing together an international training school, still funded by TU1208, held in Malta in January 2016. We then worked together again during a second TU1208

STSM, in March 2017 [20, 21]. The two institutions are now planning to present a project proposal together, in the framework of bilateral bands explicitly dedicated to Italian-Maltese collaborations.

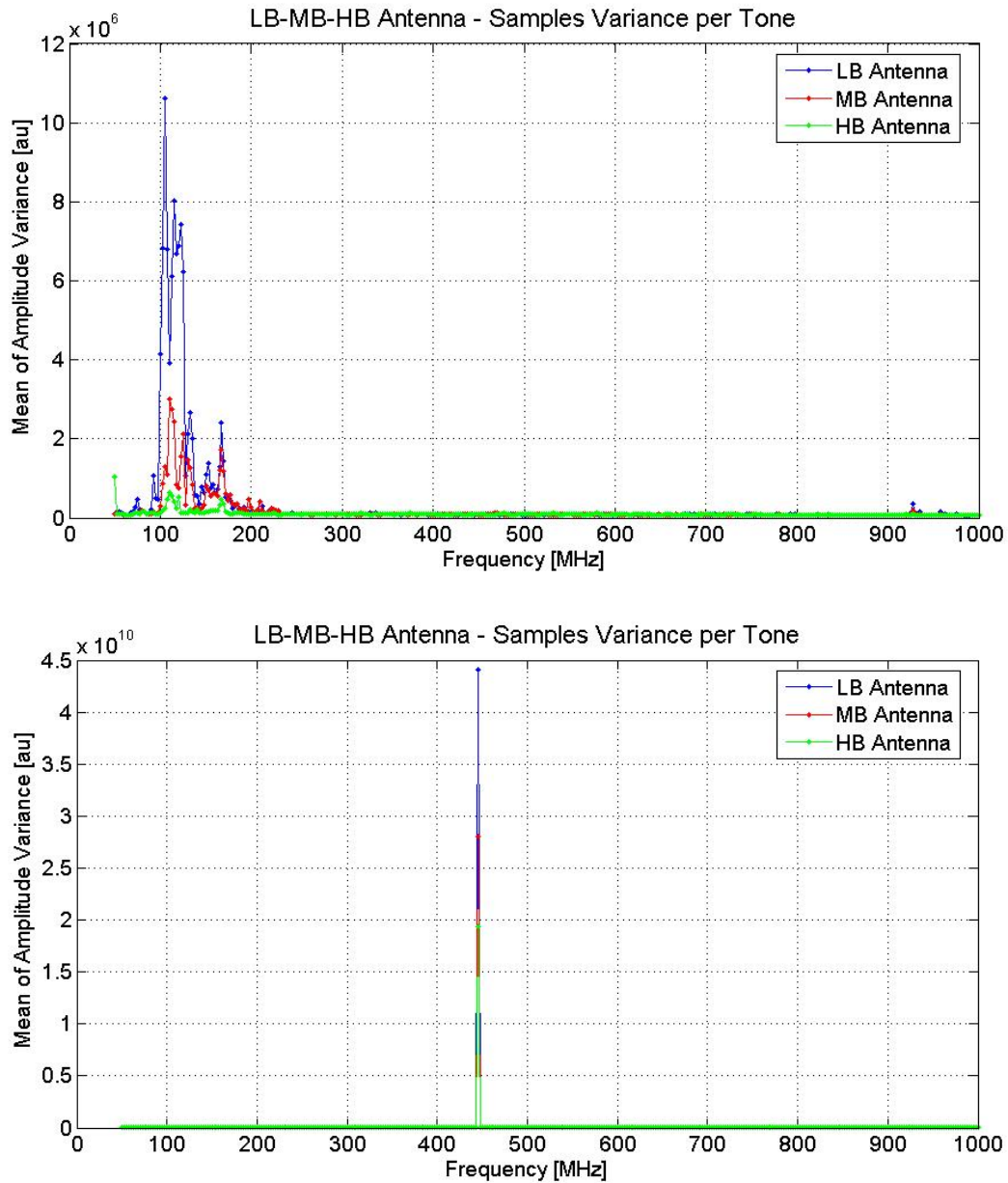


**FIG. 24** – Variance of the tones in St. John co-cathedral. Upper panel: interferences gathered with the transceivers of the staff switched off. Lower panel: interferences gathered with the transceivers switched on.



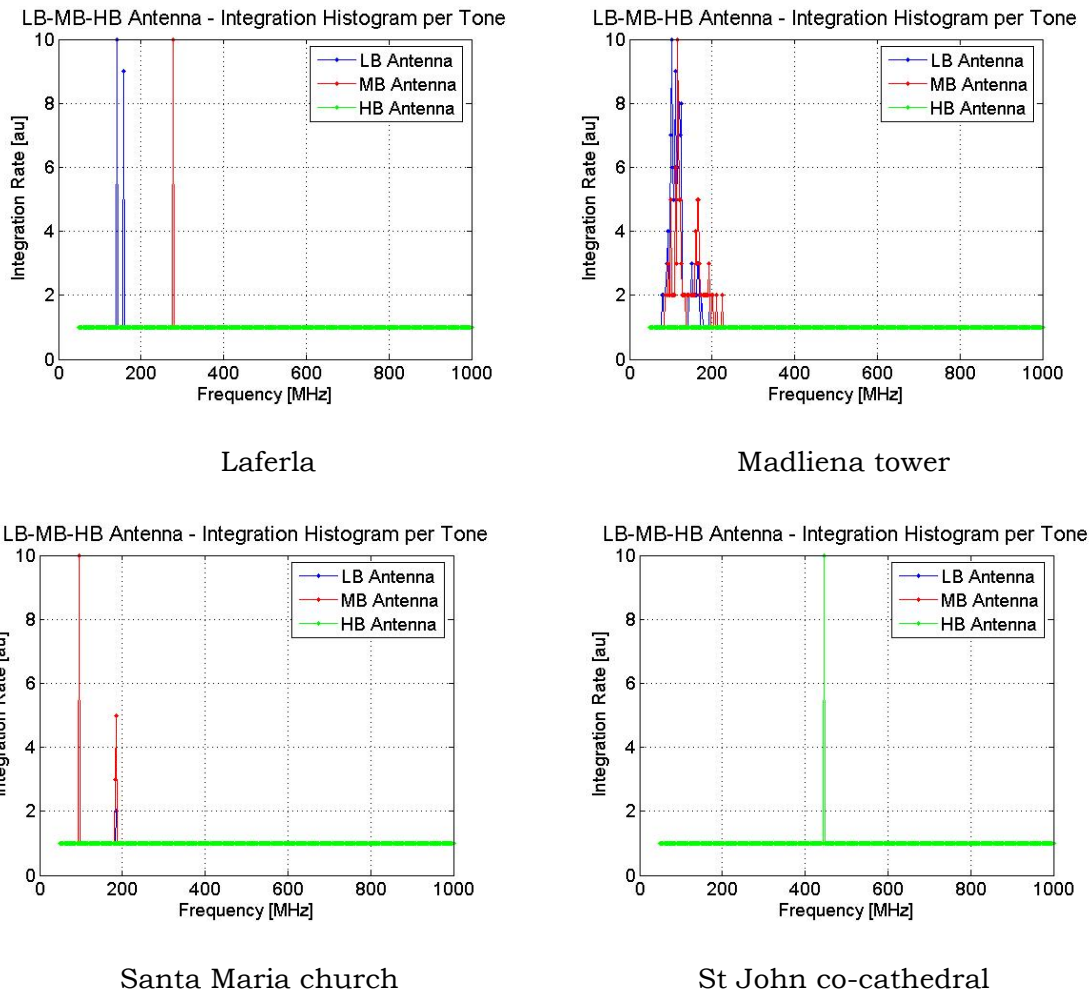


**FIG. 30** – Prolongation of the integration times for each couple of antennas and for each investigated site.

### ACKNOWLEDGEMENTS

All measurements were performed during a Short-Term Scientific Mission (STSM) funded by the COST (European Cooperation in Science and Technology) Action TU1208 “Civil engineering applications of Ground Penetrating Radar.” The authors are grateful to COST for funding and supporting the Action TU1208. The authors are also grateful to Dr Loredana Matera for helping with the elaboration of the Ground Penetrating Radar data.

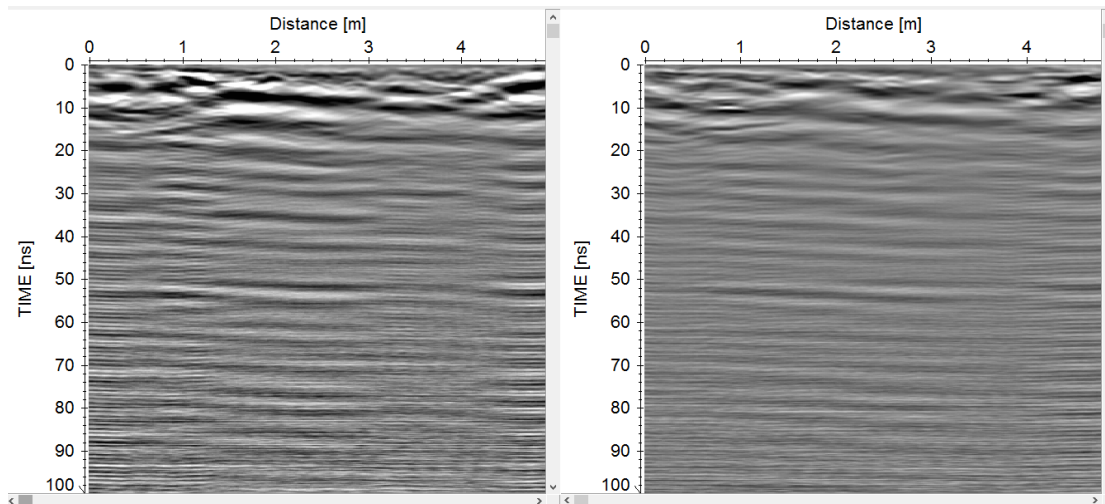


**FIG. 31** – Non-reconfigured (left hand side) and reconfigured (right hand side) B-scan. Site of Laferla Cross.

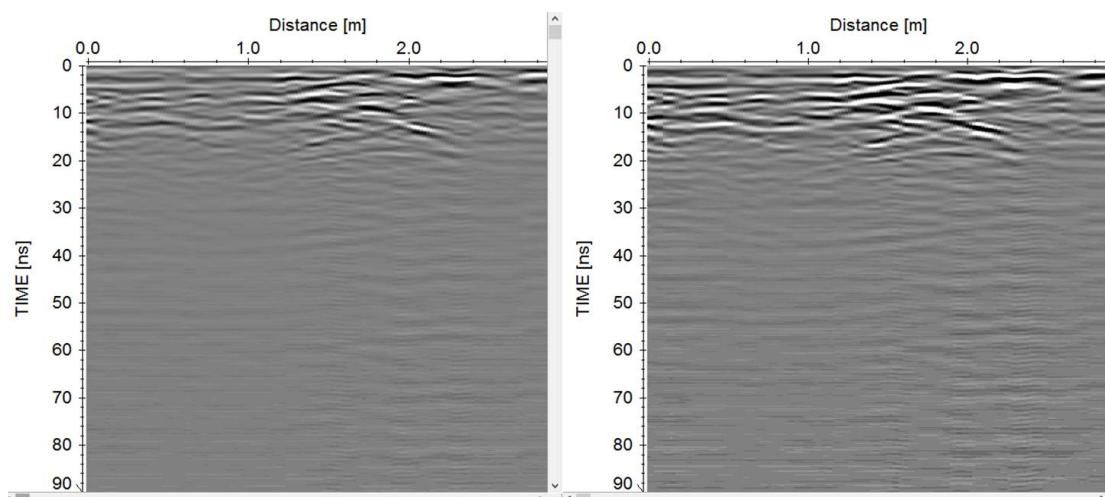


**FIG. 32** – Nonreconfigured (left hand side) and reconfigured (right hand side) Bscan. Site of Madliena Tower.

## REFERENCES

- [1] R. Persico and G. Prisco, "A Reconfigurative Approach for SF-GPR Prospecting," *IEEE Transactions on Antennas and Propagation*, vol. 56, n.8, pp. 2673–2680, 2008.
- [2] L. Matera and J. Sala, "Tests, comparison and improvement plans for an innovative reconfigurable stepped-frequency GPR," book chapter in *Short-Term Scientific Missions - Year 2*, L. Pajewski and M. Marciniak, Eds.; Publishing House: Aracne; Rome, Italy, May 2015; ISBN 978-88-548-8488-5.

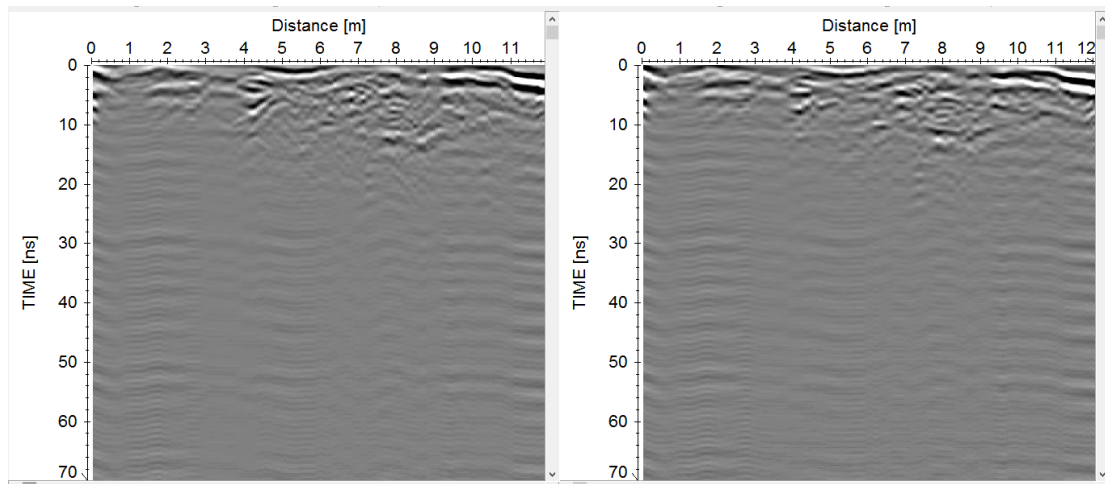


**FIG. 33** – Non-reconfigured (left hand side) and reconfigured (right hand side) B-scan. Site of Santa Maria Church.

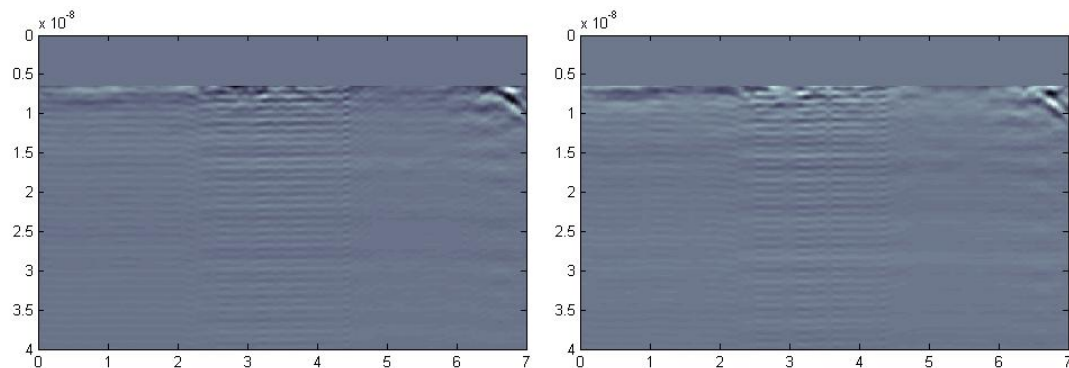


**FIG. 34** – Non-reconfigured (left hand side) and reconfigured (right hand side) B-scan. Site of the co-cathedral of St. John.

[3] R. Persico, M. Ciminale, and L. Matera, “A new reconfigurable stepped frequency GPR system, possibilities and issues; applications to two different Cultural Heritage Resources,” *Near Surface Geophysics*, vol. 12, pp. 793–801, 2014.

[4] P. Y. Bard, “Guidelines for the implementation of the H/V spectral ratio technique on ambient vibrations: measurements, processing, and interpretations,” *SESAME European Research Project, WP12, deliverable D23.12, 2004*, available at [sesame-fp5.obs.ujf-grenoble.fr/Deliverables2004](http://sesame-fp5.obs.ujf-grenoble.fr/Deliverables2004).

- [5] M. Nogoshi and T. Igarashi, "On the amplitude characteristics of microtremor (part 2)," *Journal of Seismology of the Society of Japan*, vol. 24, pp. 26–40, 1971.
- [6] Y. Nakamura, "A method for dynamic characteristics estimation of subsurface using microtremor on the ground surface," *Quarterly Report of Railway Technical Research Institute (RTRI)*, vol. 30(1), pp. 25–33, 1989.
- [7] S. Bonnefoy-Claudet, F. Cotton, and P. Y. Bard, "The nature of noise wavefield and its applications for site effects studies: a literature review," *Earth-Sci. Rev.*, vol. 79(3), pp. 205–227, 2006.
- [8] H. M. Pedley, M. R. House, and B. Waugh, "The geology of Malta and Gozo. Proceedings of the Geologists' Association," vol. 87, pp. 325–341, 1976.
- [9] M. Pedley, M. Hughes-Clarke, and P. Galea, P., "Limestone Isles in a Crystal Sea — The Geology of the Maltese Islands," Publishers Enterprises Group Ltd, San Gwann, Malta, 2002.
- [10] P. Galea, S. D'Amico, and D. Farrugia, "Dynamic characteristics of an active coastal spreading area using ambient noise measurements (Anchor Bay, Malta)," *Geophysical Journal International*, vol. 199, pp. 1166–1175, 2014.
- [11] F. Panzera, S. D'Amico, A. Lotteri, P. Galea, and G. Lombardo, "Seismic site response of unstable steep slope using noise measurements: the case study of Xemxija bay area, Malta," *Natural Hazard and Earth System Science*, vol. 12, pp. 3421–3431, 2012.
- [12] G. Gigli, W. Frodella, F. Mugnai, D. Tapete, F. Cigna, R. Fanti, and L. Lombardi, "Instability mechanisms affecting cultural heritage sites in the Maltese Archipelago," *Natural Hazards and Earth System Science*, vol. 12, pp. 1883–1903, 2012.
- [13] F. Panzera, S. D'Amico, P. Galea, G. Lombardo, M.R. Gallipoli, and S. Pace, "Geophysical measurements for site response investigation: preliminary results on the island of Malta," *Bollettino di Geofisica Teorica ed Applicata*, vol. 54(2), pp. 111–128, 2013.
- [14] A. Vella, P. Galea, and S. D'Amico, "Site frequency response characterisation of the Maltese islands based on ambient noise H/V ratios," *Engineering Geology*, vol. 163, pp. 89–100, 2013.
- [15] R. Persico, *Introduction to Ground Penetrating Radar, Inverse Scattering and Data Processing*, Wiley, 2014.
- [16] K. J. Sandmeier, *Reflexw 3.0 manual - Sandmeier Software*, Karlsruhe, Germany, 2003.

- [17] F. Soldovieri, G. Prisco, and R. Persico, "Application of Microwave Tomography in Hydrogeophysics: some examples," *Vadose Zone Journal*, vol. 7(1), pp. 160–170, 2008.
- [18] L. Mertens, R. Persico, L. Matera, and S. Lambot, "Smart automated detection of reflection hyperbolas in complex GPR images with no a-priori knowledge on the medium," *IEEE Transactions on Geoscience and Remote Sensing*, vol. 54(1), pp. 580–596, 2016.
- [19] N. Masini, R. Persico, E. Rizzo, A. Calia, M.T. Giannotta, G. Quarta, and A. Pagliuca, "Integrated Techniques for Analysis and Monitoring of Historical Monuments: the case of S.Giovanni al Sepolcro in Brindisi (Southern Italy)," *Near Surface Geophysics*, vol. 8(5), pp. 423–432, 2010.
- [20] R. Persico, S. D'Amico, E. Rizzo, L. Capozzoli, and A. Micallef, "Ground Penetrating Radar investigations in sites of cultural interest in Malta," *Ground Penetrating Radar*, vol. 1(1), pp. 38–62, 2018.
- [21] R. Persico, S. D'Amico, E. Rizzo, L. Capozzoli, and A. Micallef, "Electrical resistivity tomography investigations in Mgarr (Malta)," *Ground Penetrating Radar*, vol. 1(1), pp. 63–74, 2018.